Available online at www.sciencedirect.com
ScienceDirect
Journal of Power Sources 162 (2006) 316–326
JOURNAL OF POWER SOURCES
www.elsevier.com/locate/jpowsour

Parameter setting and analysis of a dynamic tubular SOFC model

Wei Jiang [a,*], Ruixian Fang [a], Jamil A. Khan [a], Roger A. Dougal [b]

[a] *Department of Mechanical Engineering, University of South Carolina, 300 Main Street, Columbia, SC 29208, United States*
[b] *Department of Electrical Engineering, University of South Carolina, Columbia, SC 29208, United States*

Received 23 May 2006; received in revised form 27 June 2006; accepted 28 June 2006
Available online 9 August 2006

Abstract

An improved one-dimensional dynamic model of a tubular SOFC stack capable of system simulation in the virtual test bed (VTB) simulation environment is presented in this paper. This model is based on the electrochemical and thermal modeling, accounting for the voltage losses and temperature dynamics. The modeling of an external reformer is also included in this study. A detailed parametric analysis of working conditions and cell configuration of the solid oxide fuel cell (SOFC) stack is the main focus of this paper. The following operating parameters are investigated: pressure ratio, temperature, mass flow rate, external reforming degree and stream to carbon (S/C) ratio. The cell geometric parameters studied include cell diameter and cell length. Elevated operating pressure improves the cell performance. Whereas, higher operating temperature decreases both the Nernst potential and the irreversible losses, resulting in an initial increase then a decrease in cell efficiency. It was found that a higher S/C ratio yields a lower H_2 concentration and partial pressure, which has a negative effect on the Nernst potential. Increased cell diameter is found to increase the power due to a larger activation area at the same time and due to longer current path length there is an increase in the ohmic loss. Increased length of the cell has the undesired affect of an increased pressure drop.

Keywords: Solid oxide fuel cell; SOFC; Parameter; Dynamic model; Simulation; Virtual test bed

1. Introduction

The high temperature solid oxide fuel cell (SOFC), with the advantages of its high efficiency, environmental friendliness and flexibility of usable fuel types, has been considered as one of the most promising technologies for electric energy generation. Many variations of SOFC fuel cell design are possible: such as tubular, planar and monolithic. The tubular SOFC power system (Siemens-Westinghouse Power Corporation), integrated with a gas turbine, has achieved an overall 55% efficiency [1]. The planar and monolithic SOFC technologies are frequently analyzed in the literature. The current paper focuses on an improved dynamic model for a tubular SOFC stack, and a detailed parameter analysis of operating conditions and cell geometric configurations. Parameter analysis not only shows the influence of the parameters' variance on the SOFC performance, but also identifies areas of the largest possible impact with the least effort.

In the past couple of years, several models have been developed and tested to study the design and operating conditions of SOFC stack. Most models, however, are steady state models [2–4] and are valid for only the specific operating points. Padulles et al. [5] developed a SOFC model with focus on electrochemistry and species dynamics, but temperature and heat transfer dynamics were not considered in their model. A dynamic transient SOFC model has been developed by Sedghisigarchi [6], however, their model is based on lumped capacitance model where the spatial distributions of temperature, current density and species concentration are not investigated. In addition, few studies have evaluated the effect of length of current pathway, which has significant influence on the cell diameter.

In this paper, a one-dimensional dynamic model of a tubular SOFC is presented with external reforming and system integration capabilities. Based on the electrical behavior, chemical reaction equilibrium and energy balance, the proposed model can predict the SOFC characteristics in steady states and also in transient operating states. The accuracy and reliability of the model is demonstrated by comparisons with experimental data from the literature. The distinctive feature of the current model

* Corresponding author. Tel.: +1 803 777 0838; fax: +1 803 777 0106.
E-mail address: jiangw@engr.sc.edu (W. Jiang).

0378-7753/$ – see front matter © 2006 Elsevier B.V. All rights reserved.
doi:10.1016/j.jpowsour.2006.06.086

Nomenclature

c_p	specific heat (J (mol^{-1} K^{-1}))
D_h	hydraulic diameter (cm)
E	activation energy (82 kJ mol^{-1})
E°	Nernst potential (V)
F	Faraday constant (96487 C mol^{-1})
G	Gibbs free energy (J mol^{-1})
h	enthalpy (J mol^{-1})
i	current density (A cm^{-2})
i_0	exchange current density (A cm^{-2})
i_L	limiting current (A cm^{-2})
k	pre-exponential factor (4274)
K_{shift}	equilibrium constant for the shifting reaction
p	partial pressure (bar)
m	molar number of control volume (mol)
$\dot{n}_i$	molar flow rate of species i (mol s^{-1})
Nu	Nusselt expression
$\dot{r}_{CH_4}$	conversion rate for CH_4 per unit area of the cell (mol (s^{-1} cm^{-2}))
R	Universal gas constant (8.314 J (mol^{-1} K^{-1}))
t	time (s)
T	absolute temperature (K)
Q	heat transfer (kJ)
U_f	fuel utilization
$\dot{x}$	conversion rates of CH_4 (mol s^{-1})
$\dot{y}$	conversion rates of CO (mol s^{-1})
$\dot{z}$	conversion rates of H_2 (mol s^{-1})

Greek symbols

α	electron transfer coefficient
η	efficiency
η_{conc}	concentration loss (V)
η_{Act}	activation loss (V)
η_{Ohm}	ohmic resistance loss (V)
ρ	electrical resistance (Ω)

Subscripts

a	air
ar	air in reaction
ap	preheated air
i	inlet
e	outlet
f	fuel
s	solid part

is that the model takes into consideration the variation of variables in the axial direction, as a result it can predict the cell performance more accurately. Another important feature of the proposed model is that, the concentration loss is modeled by introducing partial pressure related to limiting current and an equivalent circuit has been built to evaluate how the length of the current pathway affects the ohmic loss of a tubular SOFC. In addition, the simulation results of the model, which is dynamic in nature, can be used for performance evaluation and cell design optimization under variable operating conditions and geometric conditions.

The virtual test bed (VTB) platform provides an effective computational environment to simulate the dynamic performance of the SOFC stack [7,8]. The non-linear model equations based on electrochemistry and thermodynamics are discretized in resistive companion (RC) form for effective implementation in the VTB platform.

The paper is organized as follows. In Section 2, the system configurations, operating conditions and important assumptions of SOFC stack are presented. The model description is presented in details in Section 3. The parameter analysis of operating conditions and cell configuration are presented in Section 4. Conclusions are drawn in Section 5.

2. System configuration

Fig. 1 illustrates the system configurations of a SOFC stack implemented in the VTB simulation environment. The system consists of one SOFC stack, an external reformer, two valves, one electrical load and two thermal sinks. A methane–steam mixture is supplied to the external reformer before being delivered to the SOFC stack. The inlet pressure and temperature of fuel and air are assumed as constant and defined as user input parameters. The fuel from the external reformer and the air are channeled to the anode and cathode of SOFC, respectively. Hydrogen diffuses through the anode and reacts with oxygen ions. In the cathode, oxygen diffuses through the electrode and the free electrons are absorbed. Electrical energy is hence produced along with the generation of the heat. The electrical energy is supplied to the electrical load. Under the assumption of adiabatic conditions, a portion of the heat generated during the SOFC electrochemical reaction and SOFC internal resistance is consumed to reform the fuel, and the rest is used to heat up the gases. For simplicity, the exhaust gases from SOFC stack are channeled to the thermal sinks directly in the system modeled here. It can be noted that this high temperature gas is a prime target for energy recovery, i.e., the high temperature exhaust gases, which consist of unutilized fuel and depleted air, can be supplied to a combustor for operation of a Brayton cycle gas turbine. The detailed operating conditions and SOFC parameters used in the current study are listed in Table 1.

With a given inlet pressure, the mass flow rates of the fuel and air are controlled by adjusting the openings of two throttle valves. In the external reformer, methane participates in the reforming reaction, which produces hydrogen and carbon dioxide. The electrical load is simplified as a resistive load, whose value is treated as an input parameter and can be changed to study the behavior of the SOFC under variable load conditions. The SOFC model shown in Fig. 1 is a two-level VTB model. The first level, shown as a SOFC stack icon, includes one electrical type connector and four fluid type connectors, which are an air inlet, an air outlet, a fuel inlet and a fuel outlet respectively. It can be noted that each of the fluid type connector consists of two ports: one natural port and one signal port. The natural port is used for the variable pressure and mass flow rate while the signal port is used for temperature and species fraction. More

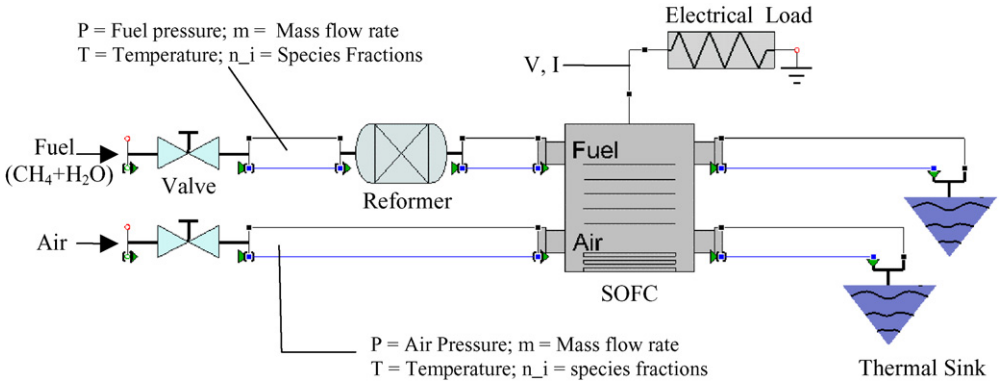

Fig. 1. Schematic diagram of SOFC stack system in VTB.

Table 1
Operating conditions and cell specifications

Parameter	Value	Unit
Operation conditions		
Stack power output	440	kW
Cell voltage	0.603	V
Average current density	0.301	A cm^{-2}
Average power density	0.182	W cm^{-2}
Air pressure ratio	5	NU
Fuel pressure rato	5	NU
Air flow rate	1.08	kg s^{-1}
Fuel flow rate	0.118	mol s^{-1}
Air inlet temperature	900	K
Fuel inlet temperature	900	K
Stack pressure loss	2	%
Fuel utilization	0.855	NU
Fuel composition	33.3% CH_4	66.7% H_2O
Cell parameters		
Number of cell	10000	
Cell area	242	cm × cm
Cell length	50	cm
electrolyte thickness	0.004	cm
Anode thickness	0.19	cm
Cathode thickness	0.01	cm

information on port definition can be found in reference [7]. By connecting the ports of SOFC with those of the models available in VTB model library, user can easily integrate the SOFC model into any specific system. Fig. 2 illustrates the second level of the SOFC model, which includes the detailed configurations of the singular cell. As shown in Fig. 2, the cell is divided into several elements along the flow direction by the finite volume method in which all the governing equations, i.e. electrochemical reaction, mass conservation and energy conservation equations, are solved for each element. The number of elements is determined by the complexity and accuracy requirement of the system and can be easily changed by the user as needed. The detailed description of the finite volume method is presented in Section 3.3.

3. Model description

A one-dimensional dynamic model of a SOFC stack, based on the earlier work [20], has been developed. The stack model has been improved significantly by introduction of an external reformer, appropriate modeling of concentration loss by introducing partial pressure related to limiting current, and most importantly, an equivalent circuit has been built to evaluate how the length of current pathway affects the ohmic loss of tubular SOFC. The following important assumptions are made in developing the SOFC model.

1. One-dimensional behavior along the stream direction.
2. Walls of the SOFC tube and external walls of the SOFC system enclosure are assumed adiabatic. There is no axial heat exchange between cells.
3. Gas distribution among cells is uniform. There is no deviation of the gas distribution among cells.
4. No gas phase reactions occur.
5. No gases leak outside of the system.
6. All gases are assumed to be ideal gas.

3.1. External reformer model

Two reactions occur in the external reformer.

$$\text{Reforming } CH_4 + H_2O(\dot{x}) \leftrightarrow CO + 3H_2$$
$$(\Delta h_r = 206.1\,\text{kJ mol}^{-1}) \quad (1)$$

$$\text{Shifting } CO + H_2O(\dot{y}) \leftrightarrow CO_2 + H_2$$
$$(\Delta h_s = -41.1\,\text{kJ mol}^{-1}) \quad (2)$$

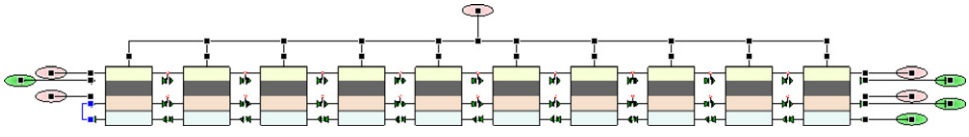

Fig. 2. Second level of the SOFC model.

Table 2
Equilibrium constant for Eq. (5)

A	B	C	D	E
5.47E−12	−2.57E−08	4.64E−05	−3.93E−02	1.32E+01

where $\dot{x}$ and $\dot{y}$ are the conversion rates of CH_4 and CO, respectively. The conversion rate $\dot{x}$ is calculated from inlet molar flow rate of methane and degree of external reforming.

$$\dot{x} = \deg_r \cdot \dot{n}^{i}_{CH_4} \tag{3}$$

where $\dot{n}^{i}_{CH_4}$ is reformer inlet molar flow rate of methane and $\deg_r$ is degree of external reforming, which is given as an input parameter.

The shifting reaction is considered to reach thermodynamic equilibrium, which can be calculated from the partial pressures of the reactants and products.

$$K_{shift}(T^e) = \frac{\dot{n}^{e}_{H_2} \cdot \dot{n}^{e}_{CO_2}}{\dot{n}^{e}_{H_2O} \cdot \dot{n}^{e}_{CO}} \tag{4}$$

The equilibrium constant for the shifting processes is temperature dependent and can be expressed as a polynomial Eq. (5)

$$\log K_{shift} = AT^4 + BT^3 + CT^2 + DT + E \tag{5}$$

where the values of the coefficients [10] are listed in Table 2.

The mass balance for the external reformer is given as:

$$\dot{n}^{e}_{CH_4} = \dot{n}^{i}_{CH_4} - \dot{x} \tag{6}$$

$$\dot{n}^{e}_{H_2} = \dot{n}^{i}_{H_2} + 3\dot{x} + \dot{y} \tag{7}$$

$$\dot{n}^{e}_{H_2O} = \dot{n}^{i}_{H_2O} - \dot{x} - \dot{y} \tag{8}$$

$$\dot{n}^{e}_{CO} = \dot{n}^{i}_{CO} + \dot{x} - \dot{y} \tag{9}$$

$$\dot{n}^{e}_{CO_2} = \dot{n}^{i}_{CO_2} + \dot{y} \tag{10}$$

The energy balance for the external reformer is given to be:

$$\sum \dot{n}_i h(T_i) = \sum \dot{n}_e h(T_e) + \dot{x} \cdot \Delta h_r + \dot{y} \cdot \Delta h_{sh} \tag{11}$$

3.2. SOFC electrochemical model

Fig. 3 illustrates the configuration and current pathway of a single tubular cell. Hydrogen diffuses through the anode and reacts with oxygen ions. In the cathode, oxygen diffuses through the electrode and the free electrons are absorbed. The electrolyte can conduct oxygen ions at temperatures above 800 °C. The anode of one cell is connected to the cathode of the next via the interconnect. Physical dimensions of each of the components are shown in Table 1.

The concerned reactions inside the cell can be summarized as follows

$$\text{Reforming } CH_4 + H_2O(\dot{x}) \leftrightarrow CO + 3H_2$$

$$(\Delta h_r = 206.1\,\text{kJ mol}^{-1}) \tag{12}$$

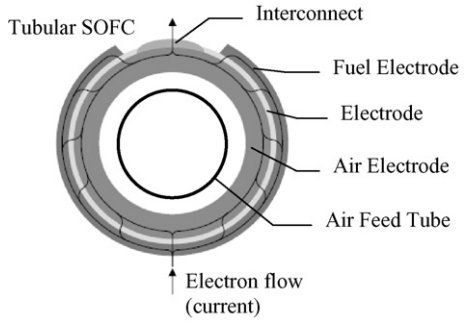

Fig. 3. Configuration and flow path of electrons and ions in a cross-section of a tubular SOFC tube.

$$\text{Shifting } CO + H_2O(\dot{y}) \leftrightarrow CO_2 + H_2$$

$$(\Delta h_s = -41.1\,\text{kJ mol}^{-1}) \tag{13}$$

$$\text{Electrochemical } H_2 + \tfrac{1}{2}O_2(\dot{z}) \rightarrow H_2O$$

$$(\Delta h_{ec} = -241.8\,\text{kJ mol}^{-1}) \tag{14}$$

where $\dot{x}$, $\dot{y}$ and $\dot{z}$ are the conversion rates of CH_4, CO and H_2, respectively. Δh_r, Δh_s and Δh_{ec} stand for reaction heat of reforming, shifting and electrochemical reactions, respectively. The reforming reaction is a highly endothermic reaction. The conversion rate $\dot{x}$ is assumed to be controlled by a conversion rate per unit area of the cell, which is named $\dot{r}_{CH_4}$ given by Achenbach [9].

$$\dot{r}_{CH_4} = k \cdot p_{CH_4} \cdot \exp\left(\frac{-E}{R \cdot T}\right) \tag{15}$$

where k is the pre-exponential factor with a value of 4274, E the activation energy of 82 kJ/mol, and p_{CH_4} is the partial pressure of methane.

Similar to the external reforming process, under the assumption that shifting reaction is always in equilibrium, the equilibrium constants can be calculated from Eq. (4).

Hydrogen conversion rate is directly related to the current, by Faraday's law.

$$z = \frac{I}{2} \cdot F \tag{16}$$

The fuel utilization coefficient U_f is given by

$$U_f = \frac{\dot{z}}{\dot{n}^{i}_{H_2} + \dot{n}^{i}_{CO} + 4\dot{n}^{i}_{CH_4}} \tag{17}$$

The cell electrical power is calculated as the product of cell current and the cell electrodes voltage. The reversible voltage calculated based on the knowledge of the cell potential from the Nernst equation.

$$E^\circ = \frac{-\Delta G^\circ}{2F} + \frac{RT}{2F} \ln \frac{p_{H_2} p_{O_2}^{1/2}}{p_{H_2O}} \tag{18}$$

where p terms are the partial pressures of reacting species, R the universal gas constant and F is Faraday constant. The change of

Gibbs free energy ΔG° is the function of temperature and can be described as a polynomial equation. The coefficients *a–c* are taken from Reid et al. [11]

$$\Delta G^\circ = aT^2 + bT + C \tag{19}$$

The Nernst potential is reduced due to the following irreversible losses:

1. concentration loss η_{conc} (V);
2. activation loss η_{Act} (V);
3. ohmic resistance loss η_{Ohm} (V).

Therefore, the actual voltage can be expressed as

$$V = E^\circ - (\eta_{\text{Act}} + \eta_{\text{Ohm}} + \eta_{\text{Conc}}) \tag{20}$$

(1) *The concentration loss* is calculated as follows [12,13]:

$$\eta_{\text{Conc}} = \frac{RT}{nF} \ln\left(1 - \frac{i}{i_{\text{L}}}\right) \tag{21}$$

where i is the cell current, i_{L} the limiting current and n is the number of electrons participating in the reaction. Accounting for the known impact of pressure on mass diffusion and experimental observation, variable i_{L} can be written as [19]:

$$i_{\text{L}} = i'_{\text{L}} \times \left(\frac{p}{p'}\right)^a \tag{22}$$

where a is a constant, p the pressure and "primed" variables are for atmospheric conditions.

(2) *The activation loss* occurs when the rate of electrochemical reaction at an electrode surface is controlled by sluggish electrode kinetics [14,15], which is shown as follows

$$\eta_{\text{Act}} = \frac{RT}{\alpha n F} \ln\left(\frac{i_{\text{den}}}{i_0}\right) \tag{23}$$

where α is the electron transfer coefficient of the reaction at the electrode and i_0 is the exchange current density, which is a function of stack temperature.

(3) According to Bessett [16], the resistivity for the different layers of tubular SOFC is given by

$$\rho = 0.008114\, e^{600/T} \quad \text{(air electrode)} \tag{24}$$

$$\rho = 0.00294\, e^{10350/T} \quad \text{(electrolyte)} \tag{25}$$

$$\rho = 0.00298\, e^{-1392/T} \quad \text{(fuel electrode)} \tag{26}$$

$$\rho = 0.12568\, e^{4690/T} \quad \text{(interconnect)} \tag{27}$$

The current pathway in a tubular SOFC is shown in Fig. 3. The current collects circumferentially around the anode and the cathode tubes; and oxide ions move perpendicularly across the electrolyte layer. To account for the ohmic loss along the circumferential pathway, an equivalent circuit shown in Fig. 4 was created to evaluate the ohmic loss. The ohmic loss for the electrolyte layer and interconnect can be given by

$$R = \rho \cdot \frac{L}{A} \tag{28}$$

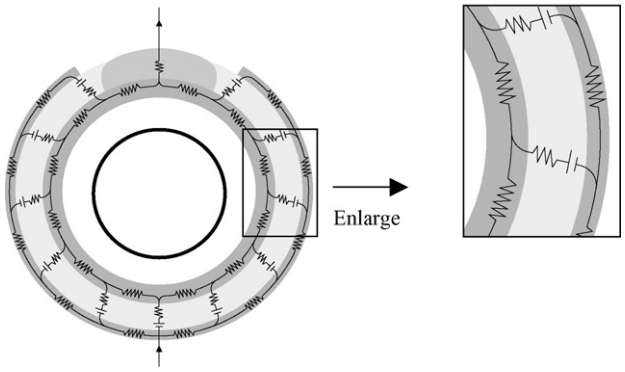

Fig. 4. Equivalent circuit for the tubular SOFC cross.

where L is the layer thickness and A is unit area. But for the anode and cathode layers, the effect of circumferential current pathway must be considered to evaluate the ohmic loss. The length of current pathway is the function of cell diameter. The influence of cell diameter is investigated by simulating the equivalent circuit in Fig. 4 with different diameters. Therefore a corrective coefficient was introduced to account for anode and cathode layer ohmic losses.

$$\zeta = \left(\frac{D}{D'}\right)^{c1} \tag{29}$$

where $c1$ is a constant, D the cell diameter and D' is the reference diameter.

The ohmic loss can be expressed as

$$\eta_{\text{Ohm}} = I \cdot R \tag{30}$$

3.3. SOFC thermal model

Fig. 5 shows the schematic configuration of a single tubular fuel cell with discretized axial elements used for heat transfer calculations. The heat released from chemical reaction and electrical resistance loss is absorbed by the solid, where it is further transferred to the fuel and air steam. The air entering from the air feed tube is pre-heated by the air in reaction. For the thermal model the following assumptions are made

1. Heat release and absorption arising from reforming, shifting, electrochemical reactions and electrical resistance occur within solid part of each cell.
2. Heat transfer between the solid and the gas steams occur by convection heat transfer. Radiation heat transfer between solid part and gas steams is not considered here. Preliminary calculation by the authors revealed that radiation heat transfer was much smaller than the convective heat transfer, as a result radiation heat transfer was neglected. The effect of radiation will be investigated in more detains in the future work.
3. The axial conduction heat transfer between nodes is neglected.
4. The cell voltage at each element is uniform.

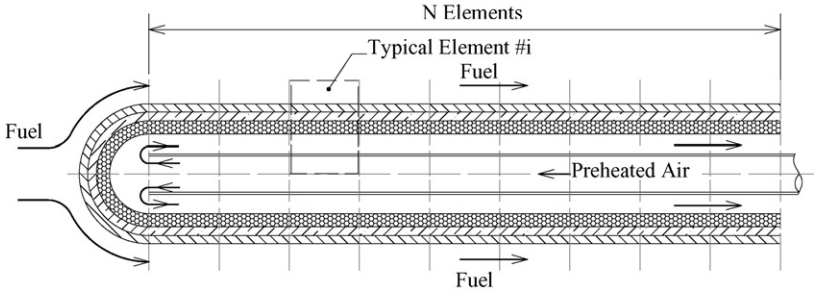

Fig. 5. Heat transfer assumption and element dividing.

As seen in Fig. 5, the cell is divided into elements along the flow direction. The temperature gradient of gas steams in the flow direction is assumed to depend only on the convection heat transfer between the channel walls and the gas stream. For each element, as shown in Fig. 6, there are four control volumes: fuel, solid, reaction air and pre-heated air. Four different temperatures T_f, T_s, T_{ar}, T_{ap}, corresponding to the temperatures of fuel, solid, air in reaction and pre-heated air, respectively, are considered within any element of each cell under the assumption of uniform temperature within each of the control volume.

For the solid control volume, the energy equation is given as

$$M_s \cdot c_p \cdot \frac{dT_s}{dt} = Q_{gen} - Q_f - Q_{ar} - W \quad (31)$$

where Q_{gen} is the total internal heat generation, Q_f and Q_{ar} the convection heat transfers to fuel and reaction air, respectively and W is the electrical power produced by the SOFC stack.

The total heat generation Q_{gen} accounting for the reactions (shifting, reforming and electrochemical) and resistance to current is given by

$$Q_{gen} = -(\dot{x} \cdot \Delta h_r + \dot{y} \cdot \Delta h_{sh} + \dot{z} \cdot \Delta h_{ec}) + I^2 \cdot \sum R_i \quad (32)$$

The electrical power is calculated as the product of current and voltage

$$W = V \cdot I \cdot N_{cell} \quad (33)$$

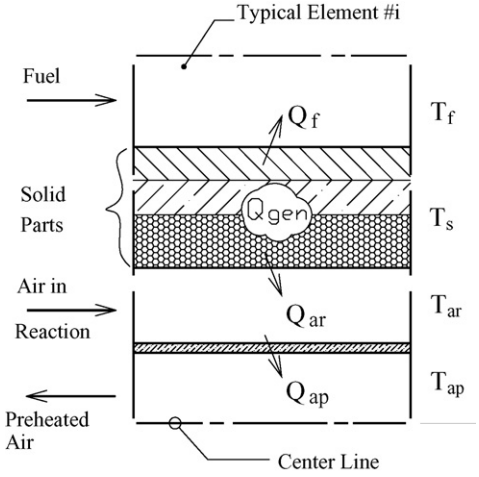

Fig. 6. Control volume defining for one element.

The convection heat transfers Q_f and Q_{ar} can be calculated by

$$Q_f = \alpha_f A_f (T_s - T_f) \quad (34)$$

$$Q_{ar} = \alpha_{ar} A_{ar} (T_s - T_{ar}) \quad (35)$$

The heat transfer coefficients α_f and α_{ar} are given by the Nusselt expression:

$$\alpha = \frac{Nu \cdot k_c}{D_h} \quad (36)$$

where Nusselt number is set to 4 according to Rokni and Yuan [17], k_c is the conductivity of the gas and D_h is hydraulic diameter.

The validity of numerical scheme used for calculating the instantaneous temperature in the gas control volume is based on a small simulation time step. For a small simulation time step (0.0001 s), the originally simultaneous process of the flow of the stream flowing and the transfer of heat can be assumed to be two separate processes, one preceding the other:

(1) Firstly, stream flows along the axial direction, as seen in Fig. 7, at a given time step some gas flows into the control volume while an amount of gas flows out into the next element. We assume each of the control volume to be well mixed (this is a valid assumption for small control volume), we can now calculate an average temperature using an energy balance. This process can be described by Fig. 7.The resulting conservation of energy equation is given by

$$h_{T_{ave}} = h_{T_{ori}} + [h_{T_{in}} - h_{T_{ori}}] \cdot \frac{\dot{n} \cdot \Delta t}{m} \quad (37)$$

where T_{in}, T_{ori} and T_{ave} are the temperatures of entering steam, exiting steam and the well mixed control volume,

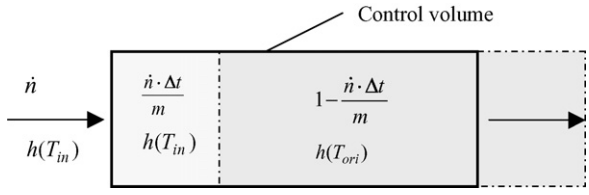

Fig. 7. Gas control volume.

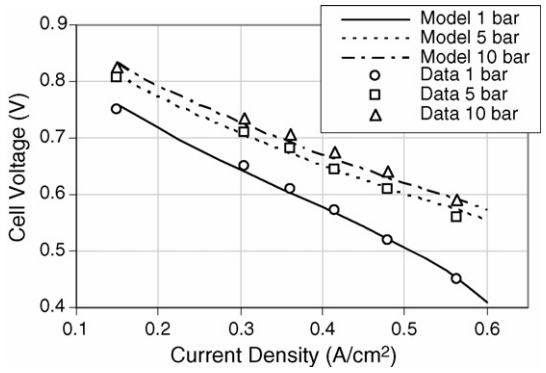

Fig. 8. Comparison of experimental data [18] with model, parametric pressure variation fuel: 89% H_2, 11% H_2O, 85% fuel utilization; operating temperature: 1000 °C.

respectively. $\dot{n}$ the molar flow rate, Δt is the simulation time step and m is the molar number of control volume.

(2) Heat transfer occurs after the mixing. The energy equations for gaseous control volumes can be calculated by

$$\text{fuel } m_f c_p \frac{dT_f}{dt} = Q_f \tag{38}$$

$$\text{reaction air } m_{ar} c_p \frac{dT_{ar}}{dt} = Q_{ar} - Q_{ap} \tag{39}$$

$$\text{preheated air } m_f c_p \frac{dT_{ap}}{dt} = Q_{ap} \tag{40}$$

The SOFC stack efficiency is given by Eq. (41), where W is the electric power. LHV is the lower heating value of inlet fuel.

$$\eta_{Overall} = \frac{W}{LHV} \tag{41}$$

4. Parameter analysis

The parameter analysis of tubular SOFC, based on the design point listed in Table 1 and system shown in Fig. 1, will be presented in this section. The following operating parameters are investigated:

- Stack pressure ratio (operation pressure to atmosphere pressure).
- Temperature, including stack mean temperature, air inlet temperature and fuel inlet temperature.
- Mass flow rate, including air flow rate and fuel flow rate.
- Degree of external reforming.
- Stream to carbon (S/C) ratio.

The cell geometric parameters studied include:

- diameter of the tubular SOFC, and
- length of the tubular SOFC.

It should be pointed out that all the calculations are made at the design point with following input parameters: the temperature of fuel and air, the flow rate of fuel and air and cell geometry, which are kept constant unless mentioned specifically.

4.1. Pressure ratio

Fig. 8 shows the comparisons between simulation results and experimental data [18] for *I–V* characteristics curve at the operating pressures ratio of 1, 5 and 10. A very good agreement is obtained throughout the test range. For the sake of comparing with the experimental conditions, the fuel composition is set to 89% H_2, 11% H_2O, with 85% fuel utilization. The mean operating temperature is set at 1000 °C by adjusting the air flow rate.

Under the simulation conditions listed in Table 2, the effects of operating pressure on the cell voltage and efficiency is shown in Fig. 9(a). As operating pressure increases, the cell voltage and efficiency increase because of the increased Nernst potential and lower concentration loss. When operating pressure ratio increases from 1 to 15, an improvement of 7.38% and 24.17% is obtained for the cell voltage and efficiency, respectively. However, the improvement of cell voltage and efficiency is not a linear function of the increase of pressure. After an initial increase the increase is less with further increase in pressure. This is due to the fact that the pressure contribution to the Nernst potential is logarithmic in nature. The solid temperature profile under various operating pressures is shown in Fig. 9(b). It is obvious that the temperature profile becomes sharper with higher pressure. The temperatures of the solid near exit are nearly the same for different operating pressure while there is a big increase in maximum temperature for the higher pressure. Given a constant fuel and air mass flow rate, a higher pressure leads to a better cell efficiency and fuel utilization, resulting in a bigger amount of

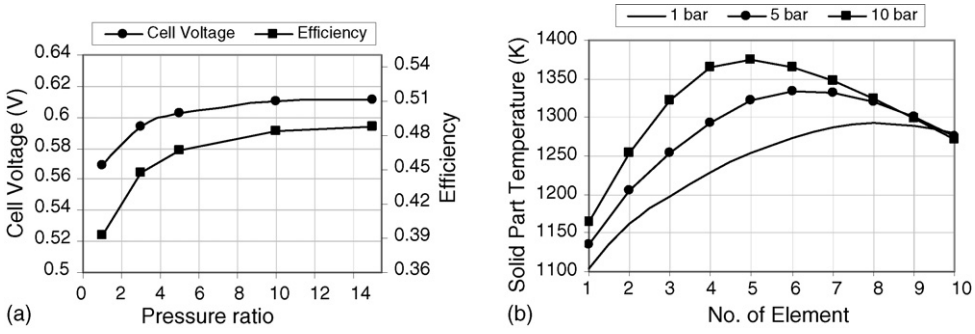

Fig. 9. Effect of stack pressure on the: (a) cell voltage and efficiency; (b) solid part temperature profile.

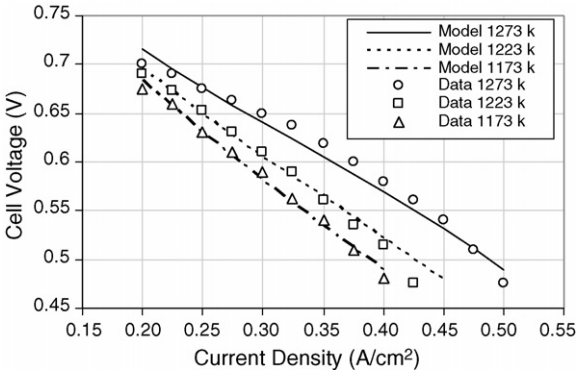

Fig. 10. Comparison of experimental data [21] with model, parametric operating temperature variation fuel: 89% H_2, 11% H_2O, with 85% fuel utilization.

fuel taking part in the reaction in the inlet. As a result, there is a steeper rise in the temperature for the higher pressure due to the fact that more heat is generated

4.2. Temperature

4.2.1. Stack temperature

The mean stack temperature is adjusted and kept to 1173, 1223 and 1273 K by changing the air mass flow rates in order to validate the comparison with the experimental data [21]. The fuel composition for this comparison is 89% H_2, 11% H_2O, with 85% fuel utilization.

As shown in Fig. 10, the agreement is very good (<1.5%) for the whole 1173 K case and good for the lower current density part of the 1223 K case. For the 1273 K case and exit side for the 1223 K case, relatively higher variance may be due to an overestimation of the activation loss and the simplification of the SOFC geometry. However, the trend of the simulated *I–V* characteristics matches well with that of the experimental data. Moreover, the maximum relative discrepancy between the model and the experiment results are below 5%, showing a fairly good fit. Along with the comparison for pressure in Section 4.1, it can be validated that the proposed SOFC model indeed works well to predict the overall performance of a tubular SOFC.

4.2.2. Air inlet temperature

The effect of air inlet temperature on the SOFC performance is shown in Fig. 11(a and b). The air inlet temperature is varied and all the other input parameters are kept constant. As a matter of fact, the impact of air inlet temperature variance on SOFC performance is caused by the solid part temperatures changes due to the varied air inlet temperature. As shown in Fig. 11(b), the mean solid temperature increases from 1180 to 1390 K when the air inlet temperature rises from 600 to 800 K. The reduction of irreversible losses while operating under higher temperature leads to a better performance in terms of cell voltage, U_f and efficiency. Therefore the voltage, U_f and efficiency rise at first. However, this effect is completely cancelled out by a further reduction of Nernst potential because of the higher temperature. Therefore, cell voltage, U_f and efficiency increase initially as the air temperature is increased and then decrease with the increase of air inlet temperature (when the decrease in Nernst potential is greater than the corresponding reduction in the irreversible losses).

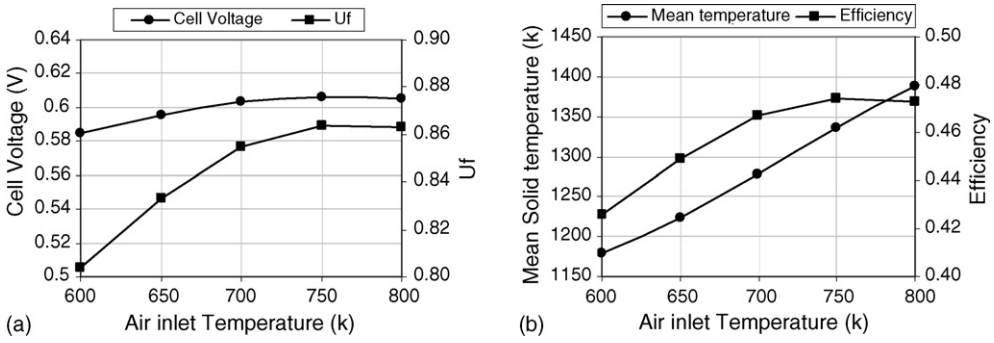

Fig. 11. Effect of air inlet temperature on the: (a) cell voltage and U_f; (b) mean temperature and efficiency.

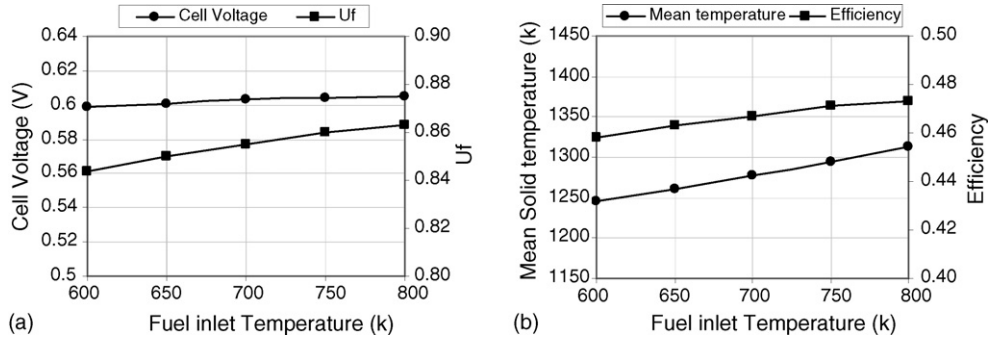

Fig. 12. Effect of fuel inlet temperature on the: (a) cell voltage and U_f; (b) mean temperature and Efficiency.

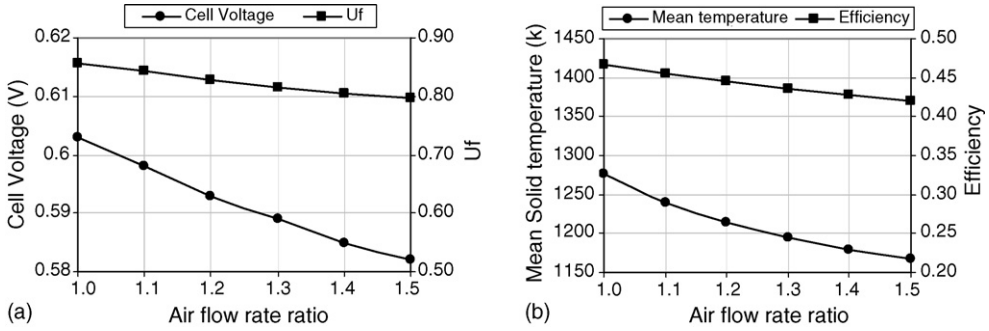

Fig. 13. Effect of air flow rate ratio on the: (a) cell voltage and U_f; (b) mean temperature and efficiency.

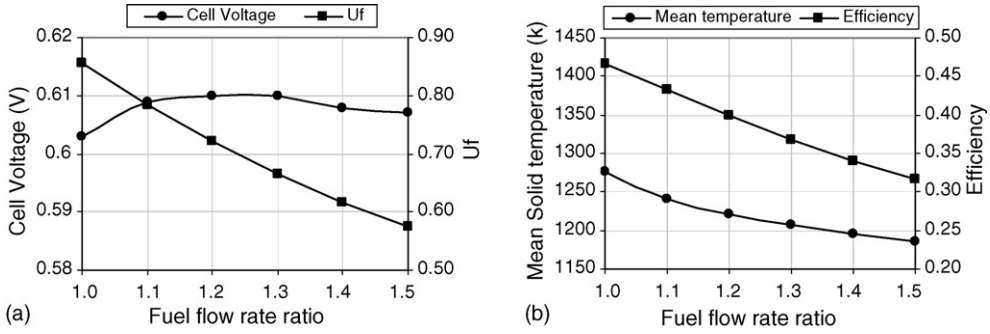

Fig. 14. Effect of fuel flow rate ratio on the: (a) cell voltage and U_f; (b) mean temperature and efficiency.

4.2.3. Fuel inlet temperature

The effect of fuel inlet temperature on the SOFC performance is shown in Fig. 12(a and b). Because of a relatively lower mass flow rate of fuel, there is a minor influence on the cell performance when the fuel inlet temperature is changed. As shown in Fig. 12(b), there is only a total increase of 68 K in the mean temperature when fuel inlet temperature rises from 600 to 800 K. In this small range of operating temperature, the effect of reduction in irreversible losses overcomes the influence of the reduction in Nernst potential. So the cell performance in terms of cell voltage, U_f, and efficiency is improved with the increasing of fuel inlet temperature.

4.3. Mass flow rate

4.3.1. Air flow rate

Fig. 13(a and b) show the curves of cell voltage, U_f, mean solid temperature and efficiency via the air flow rate ratio. The simulation begins from the operating condition listed in Table 2. The other input parameters are kept constant while air flow rate is increased by 10%, 20%, 50% by adjusting the opening of the control valve in the testing system. The solid temperature decreases because of the cooling effect of larger amount of air. The decreased temperature yields to a lower cell voltage, U_f and lower cell efficiency.

4.3.2. Fuel flow rate

Similar to the effect of increasing air flow rate, higher fuel flow rate yields a decreased mean solid temperature as shown in Fig. 14(b). With increasing of fuel flow rate, U_f, and efficiency decreases quickly as shown in Fig. 14(a and b); this is because fuel can only be partially oxidized. The cell voltage increases initially because of a higher amount of fuel participating in the reaction. But this effect will be overcome later due to the cooling effect of higher fuel flow rate. Therefore, cell voltage increase at first and then decrease with the increase of fuel flow rate.

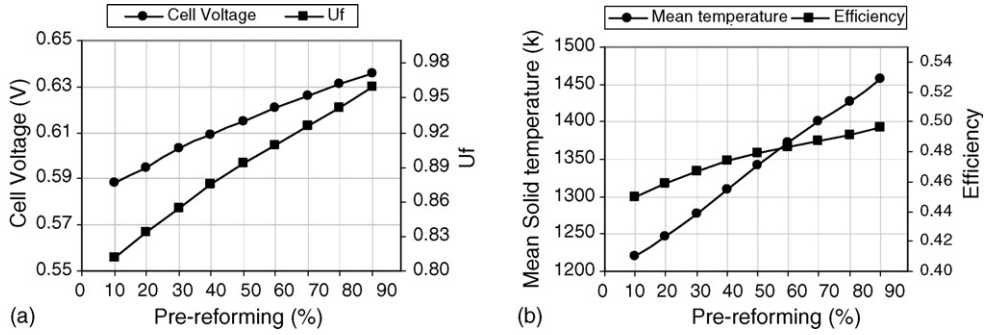

Fig. 15. Effect of external reforming on the SOFC performance. (a) Cell voltage and U_f; (b) mean temperature and efficiency.

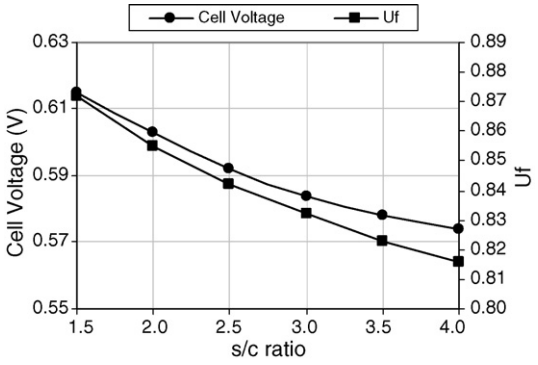

Fig. 16. Effect of S/C ratio on the cell voltage and U_f.

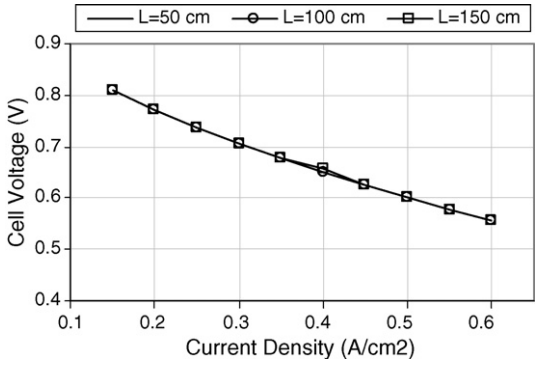

Fig. 18. Effect of length of tubular SOFC on the cell voltage.

4.4. Degree of external reforming

The effect of degree of external reforming on the SOFC performance is shown in Fig. 15(a and b); with a degree variation from 10% to 90%. The mass flow rate of fuel and air and the inlet temperature of fuel and air are kept constant. The effect of internal reforming is weak with increasing the degree of external reforming because less and less methane will be reformed inside of the SOFC. With increasing degree of external reforming, there is less CH_4 undergoing reforming inside of SOFC and accordingly less endothermic reforming reactions. As a result, the mean solid temperature increases. The cell performance in terms of cell voltage, U_f, and efficiency benefits from the higher mean solid temperature, as shown in Fig. 15(a and b).

4.5. S/C ratio

The effect of stream to carbon (S/C) ratio on the SOFC performance is shown in Fig. 16. The S/C ratio is adjusted from 1.5 to 4, but the mass flow rate of methane is kept constant by adjusting the opening of the control valve. As shown in Fig. 16, the cell voltage and U_f decreases due to the increase of S/C ratio. The reason for this lies in the fact that the higher S/C ratio yields a lower H_2 concentration and partial pressure, which has negative effect on the Nernst potential.

4.6. Diameter of the tubular SOFC

Three different diameters: $D = 15.88$, 18 and 22 mm are investigated. The diameter of the tubular SOFC is adjusted by changing the diameter of air inlet tube listed in Table 2. The thicknesses for different layers are kept constant. U_f and mean solid temperature are fixed throughout the analysis. As suggested earlier in Section 3.2 regarding ohmic losses, increasing the diameter of tubular SOFC leads to an undesired increase in the current path length which in turn yields a higher ohmic loss, resulting in an decrease in the Nernst potential of the cell. The diameter of the SOFC has less effect on the activation and concentration losses. Fig. 17(a) shows the effect of diameter variation on the cell voltage. Obviously, for a given current density, a higher cell voltage can be obtained with a smaller diameter. As shown in Fig. 17(b), a larger diameter SOFC produces a higher output power due to the increased cell area. However, the power density of a larger diameter case is smaller than that of smaller diameter case.

4.7. Length of tubular SOFC

The effect of cell length on the SOFC performance is shown in Fig. 18. Three cases are investigated, with $L = 50$, 100 and 150 cm, respectively. Similar to the diameter analysis, the thicknesses for different layers are kept constant. U_f and mean solid temperature are fixed throughout the analysis. The three V–I curves overlap with one another, which reveals that, unlike the variation in diameters, length has no effect on the cell voltage for a given current density because it does not change the current path length. But the total power output increases because of the larger cell reaction area. In the simulation, the pressure drop inside the SOFC is given and kept constant. However, in reality, the effect of pressure drop inside the SOFC is enhanced due to the higher mass flow rate. So the diameter of cell has

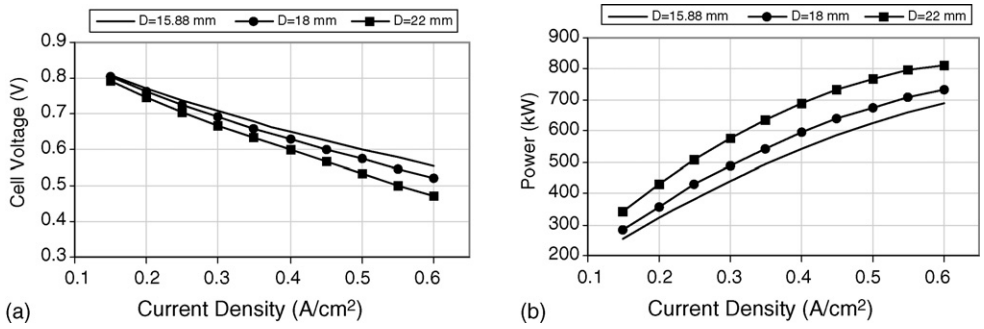

Fig. 17. Effect of diameter of tubular SOFC on the: (a) cell voltage; (b) power.

to be increased to counteract the pressure drop effects, which will have the undesired effect of increased current path length resulting in increased cell ohmic resistance.

5. Conclusions

A one-dimensional dynamic SOFC model, based on the electrochemical and thermal modeling, has been successfully developed and simulated in the VTB simulation environment. Comparisons between the simulation results and the experimental data, under different operating pressures and temperatures, demonstrate the accuracy and reliability of the model. A detailed parameter analysis of stack working condition and cell configurations of the SOFC stack is presented in this study. Listed below are the conclusions derived from the present simulation efforts:

- Elevated operating pressures can improve the cell performance in terms of cell voltage, U_f and efficiency. However, the improvement of cell performance is not linear with respect to the increase of pressure due to the fact that the pressure contribution to the Nernst potential is logarithmic in nature.
- Operating temperature plays a significant role in two important cell performances: Nernst potential and irreversible losses. Increase in operating temperature causes a reduction in irreversible losses and also in the Nernst potential. These two have opposite effects on cell voltage and its efficiencies. Therefore, cell voltage and efficiency increase initially and then with further increase in temperature the beneficial effect of lower irreversible losses is completely offset by the decrease in Nernst potential, resulting in a lower efficiency.
- The mass flow rates of air and fuel affect the cell performance due to the cooling effects of different flow rates. However, the cell performance can benefit from the larger amount of fuel because more hydrogen can be oxidized. The overall influence of fuel increase is controlled by the above two effects.
- Under the assumption of fixed fuel input temperature of the SOFC, the mean solid temperature and hydrogen concentration of the inlet fuel will increase with the increase in the degree of reforming, which improves the cell performance in terms of cell voltage and efficiency.
- For the S/C ratio, higher S/C ratio yields a lower H_2 concentration and partial pressure, which has a negative effect on the Nernst potential.
- Increase in cell diameter will increase the total power output because of the larger activation cell area, however, it yields an undesirable increase in the current path length and accordingly a higher ohmic loss. Therefore, Nernst potential and the power density of cell both decrease.
- The length of the cell has no effect on the cell voltage-current density relation curve, but the total power output increases because of the larger cell reaction area. However, the diameter of the cell has to be increased to counteract the pressure drop effects for the larger cell length, leading to an undesirable effect of increase in the current path length and thereby in the cell ohmic resistance.

Acknowledgements

The authors would like to acknowledge Office of Naval Research (ONR) and the ESRDC consortium for their financial support.

References

[1] J.H. Hirschenhofer, D.B. Stauffer, R.R. Engleman, M.G. Klett, Fuel Cell HandBook, fourth ed., Parsons Corporation, Reading, PA, 1998, for U.S. Department of Energy, November.
[2] S.H. Chan, H.K. Ho, Y. Tian, Modeling of simple hybrid solid oxide fuel cell and gas turbine power plant, J. Power Sources 109 (1) (2002) 111–120.
[3] S.H. Chan, H.K. Ho, Y. Tian, Multi-level modeling of SOFC-gas turbine hybrid system, Int. J. Hydrogen Energy 28 (2003) 889–900.
[4] A. Lazzaretto, A. Toffolo, F. Zanon, Parameter setting for a tubular SOFC simulation model, ASME 126 (March) (2004).
[5] J. Padulles, G.W. Ault, J.R. McDonald, An integrated SOFC plant dynamic model for power system simulation, J. Power Sources (2000) 495–500.
[6] K. Sedghisigarchi, Dynamic and transient analysis of power distribution systems with fuel cells—part I: fuel-cell dynamic model, IEER Trans. Energy Conversion 19 (June) (2004).
[7] G. Cokkinides, B. Beker, VTB Model Developer's Guide [online]. Available: http://vtb.engr.sc.edu/modellibrary/modeldev.asp.
[8] W. Jiang, J. Khan, R.A. Dougal, Dynamic centrifugal compressor model for system simulation. J. Power Sources, 2005, in press.
[9] E. Achenbach, Three dimensional and time dependent simulation of a planar solid oxide fuel cell stack, J. Power Sources 49 (1994) 333–348.
[10] U.G. Bossel, Final Report on SOFC Data Facts & Fig.s, Swiss Federal Office of Energy, Berne, CH, 1992.
[11] R.C. Reid, J.M. Prausnitz, B.E. Poling, The Properties of Gases and Liquids, McGraw-Hill, New York, 1987.
[12] D.J. Hall, R.G. Colclaser, Transient modeling and simulation of tubular solid oxide fuel cells, IEEE Trans. Energy Conversion 14 (Sept. 1999).
[13] L.J. Blomen, M.N. Mugerwa, Fuel Cell Systems, Plenum, New York, 1993.
[14] Fuel Cell HandBook, fifth ed., EG&G Services Parsons Inc., U.S. Department of Energy, 2000.
[15] M.D. Lukas, K.Y. Lee, H. Ghezel-Ayagh, An explicit dynamic model for direct reforming carbonate fuel cell stack, IEEE Trans. Energy Conversion 16 (September) (2001).
[16] N.F. Bessett, Modeling and Simulation for Solid Oxide Fuel Cell Power Systems. Ph.D. Thesis 1994.
[17] J. Yuan, M. Rokni, B. Sundén, The development of heat transfer and gas flow modeling in the solid oxide fuel cells, in: S.C. Singhal, M. Dokiya (Eds.), Solid Oxide Fuel Cells (SOFC VI), The Electrochemical Society, USA, 1999, pp. 1099–1108.
[18] J.H. Hirschenhofer, D.B. Stauffer, R.R. Engleman, M.G. Klett, Fuel Cell Handbook, fourth ed., FETC, Morgantown, WV, 1998.
[19] J.E. Freech, J.W. Pratt, J. Brouwer, Development of a Solid-Oxide Fuel Cell/Gas Turbine Hybrid System Model for Aerospace Applications Turbo Expo, ASME, 2004.
[20] W. Jiang, R. Fang, R.A. Dougal, J. Khan, Thermo-electric model of a tubular SOFC for dynamic simulation, J. Energy Resour. Technol., ASME, 2006, submitted for publication.
[21] S.C. Singhal, K. Kendall, High Temperature Solid Oxide Fuel Cells—Fundamental, Design and Applications, Elsevier Ltd., 2003.